Int. J. Heat Mass Transfer. Vol. 16, pp. 1231–1244. Pergamon Press 1973. Printed in Great Britain

HEAT TRANSFER TO A CYLINDRICAL LAMINAR LIQUID JET EJECTING INTO A GAS

RICHARD D. KAPLAN* and LAWRENCE H. SHENDALMAN†
Yale University, New Haven, Connecticut, U.S.A.

(*Received* 20 *April* 1971 *and in revised form* 26 *June* 1972)

Abstract—The experimentally determined heat transfer to a vertical cylindrical laminar liquid jet ejecting into a gas bath, where the resistance to heat transfer in the gas phase is controlling, is compared with that predicted by the Pohlhausen–von Karman technique, using logarithmic profiles to solve the mass, momentum, energy, and diffusion equations.

The theoretical solution was derived for the case of negligible bulk flow (as compared to the Reynolds flux) at the surface, rapid radial heat conduction, and small jet temperature change, and agreed with the experimental data, provided that the jet radius was sufficiently small. It is shown that the solution, which includes the effects of evaporation or condensation, can be put into the form of a universal plot of dimensionless axial temperature change versus dimensionless axial distance.

NOMENCLATURE

b, non-dimensional parameter which determines the error involved in neglecting the surface bulk flow, see equation (20);
B, non-dimensional coefficient defined by equation (2);
c, total molar concentration;
c_p, heat capacity at constant pressure;
C, constant, defined by equation (A.10);
C_A, modified concentration of component $A = c_A - c_{A_\infty}$;
Cn, $\Delta H_v(c_{A_i} - c_{A_\infty})/(\rho_1 c_{p_1}\{T_i - T_\infty\})$;
D, constant, defined by equation (A.13);
D_{AB}, mass diffusivity of A in B;
ΔH_v, heat of vaporization or condensation;
k, thermal conductivity;
K, variable defined by equation (A.2);
m, mass fraction;
N, molar flux;
Nu, local Nusselt number;
N_{Re_R}, Reynolds number$_R$;
N_{Re_z}, Reynolds number$_z$;
Pr, Prandtl number;
Q, $(c_A - c_{A_\infty})/(c_{A_i} - c_{A_\infty})$;
Q', rate of heat transfer per unit length;
r, radial direction;
R, radius;
Sc, Schmidt number;
T, temperature;
ΔT, temperature difference;
U, axial jet velocity;
V_r, radial velocity;
V_z, axial velocity;
x, mole fraction;
y, distance from the jet edge;
z, axial distance.

Greek symbols

α, thermal diffusivity;
γ, non-dimensional coefficient, defined by $\theta/\theta_s = 1 - (1/\gamma)\ln(1 + (y/R))$;
ε, non-dimensional axial distance;
θ, modified temperature $= T - T_\infty$;
ν, kinematic viscosity;
ρ, density;
χ, non-dimensional coefficient defined by equation (22);
Ψ, $(T - T_\infty)/(T_i - T_\infty)$;
Γ, non-dimensional coefficient, defined by: $C_A/C_{A_S} = 1 - (1/\Gamma)\ln(1 + \{y/R\})$;

* Present address: American Oil Company, Research and Development Department, 2500 New York Avenue, Whiting, Indiana 46394, U.S.A.
† Present address: Esso Research and Engineering Company, Post Office Box 45, Linden, New Jersey 07036, U.S.A.

Y, arbitrary function of z;
Ω, non-dimensional temperature change defined by equation (21).

Subscripts

A, liquid component;
B, gaseous component; bottom;
g, property at a distance into the gas phase;
i, initial;
l, liquid property;
M, methanol;
S, jet surface;
sat, saturation value;
T, top;
∞, property outside of its own boundary layer.

Superscript

$\bar{}$, average property.

INTRODUCTION

IT IS proposed that the approximate integral solution to the problem of heat transfer in the boundary layer on a constant surface temperature continuous cylinder may be applied to determine the axial temperature profile in a thin (gas phase heat transfer resistance controlling) laminar liquid jet. A volatile liquid jet is considered, necessitating solution of the diffusion equation simultaneously with the mass, momentum, and energy equations. (Experimental temperatures and driving forces were chosen such that the phase change (evaporation or condensation through the boundary layer) was the dominant contribution to the heat transferred, although convection and conduction accounted for up to 30 per cent of the heat transferred. Thus, a range of liquid volatility was simulated. Non-volatile liquid jets were not used as they would have been difficult to handle within experimental accuracy, due to the small jet temperature change expected (within experimental temperature limitations) in the absence of evaporation or condensation.)

Since the pioneering paper by Sakiadis [1] on continuous moving solid surfaces was published, numerous articles on continuous surfaces have been written [2–11]. (Examples of continuous moving surfaces are filaments continuously extruded from dies or cooled in melt or solution spinning, threads travelling between feed and wind-up rolls, and wires in leaching operations.) In almost all cases—except [5] and [6]—constant surface temperature is assumed and phase change effects are neglected. The Pohlhausen–von Kármán approximate integral method of solution is usually utilized.

In this paper use of previous work on the continuous solid cylinder (refer to [2] and [8]) is made in order to determine the axial temperature profile for a thin, continuous cylindrical liquid jet undergoing small temperature changes, and experimental confirmation is presented. Following Erickson, Fan and Cha [5], the procedure is easily extended (refer to [12]) to handle large temperature changes using average physical properties for non-volatile cylindrical liquid jets or solid cylinders.

The growth of the boundary layers is depicted in Fig. 1a. Previous studies have shown that the radial temperature profile in the jet may be assumed to be flat, provided that the jet is thin [13]; that the jet velocity profile in the radial direction may be assumed to be flat, beginning a short distance from the orifice [14]; and that there is a velocity-dependent regime in which the jet does not break up, but remains smooth.

The occurrence of condensation or evaporation has a profound influence on the amount of heat transferred. In a cooling run, the initially warmer liquid heats up the gas in the immediate vicinity of the jet. Thus, whether the gas was initially unsaturated or completely saturated (with the liquid's vapor), it becomes less than 100 per cent saturated during the course of a run. Thus, evaporation occurs. The evaporative heat requirement is given up by the liquid, further reducing its temperature. Therefore, in this case the convective–conductive effect and the evaporative effect work in the same temperature direction.

The situation is more complicated in the

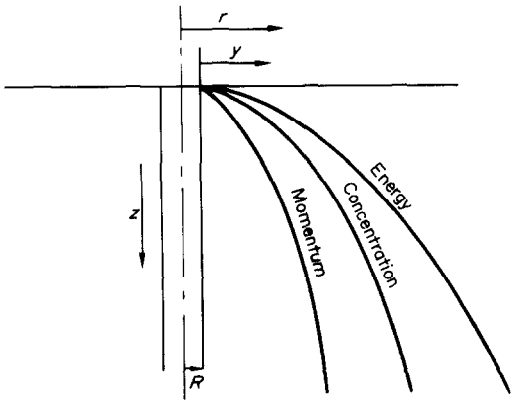

FIG. 1a. Diagram showing the coordinates and depicting the growth of the boundary layers.

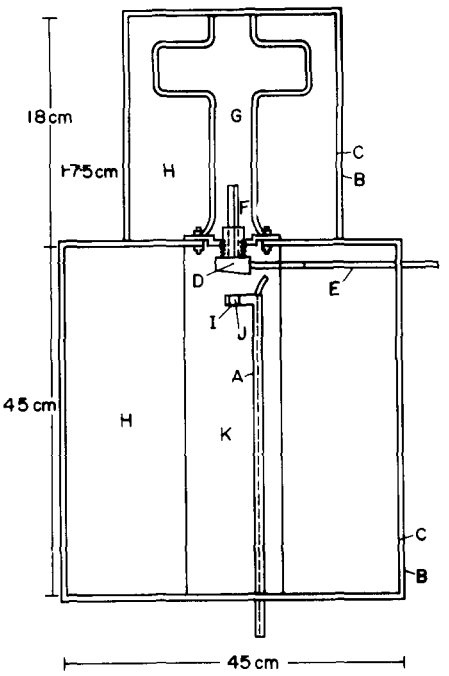

FIG. 1b. Schematic diagram of the apparatus, where: A = Teflon-covered hollow Bakelite rod, B = insulation, C = Lucite, D = Teflon blocking device, E = threaded rod, F = capillary tube, G = liquid reservoir, H = water bath, I = Teflon cup, J = thermocouple bead, K = gas bath.

heating case, however. Two distinct possibilities arise. If the gas is initially 100 per cent saturated (with the liquid's vapor), the cooler liquid lowers the temperature of the gas in the immediate vicinity of the jet. This air is thus super-saturated and condensation occurs on the jet. In this case the heat of condensation is transferred to the liquid, further heating the jet. Therefore, both driving forces are again in the same direction.

Should the gas initially be incompletely saturated at the initial temperature of the jet, condensation can not occur. Instead, evaporation occurs, withdrawing heat from the jet. Therefore, in this case the driving forces are in opposing directions. If the evaporative effect dominates, the jet cools during a "heating" run. Thus, accurate determination of the amount of condensation or evaporation is essential, as will be shown later.

THEORETICAL MODEL

Assuming that the bulk flow contribution is negligible, that the boundary layer assumption is applicable, and that a logarithmic axial gas velocity profile is appropriate, Sakiadis [2] utilized the Pohlhausen–von Kármán technique to determine that for continuous cylindrical jets:

$$\int_0^B \frac{Be^{2B} - e^{2B} + B + 1}{B^2}\, dB = \frac{2N_{Re_z}}{N_{Re_R}^2} \qquad (1)^*$$

where B is a non-dimensional coefficient that is a function of z only and is defined by

$$\frac{V_z}{U} = 1 - \frac{1}{B}\log\left(1 + \frac{y}{R}\right). \qquad (2)$$

If $Pr \leqslant 1$, the following expression derived by Rotte and Beek [8] for constant surface temperature and a similar expression for constant surface concentration apply to continuous cylinders:

* Relevant coordinates and nomenclature are shown in Fig. 1a and/or in the Table of Nomenclature.

$$\frac{\partial \gamma}{\partial \varepsilon} = \frac{\dfrac{\varepsilon B}{2Pr} - \dfrac{B^2\left(\dfrac{N_{Re_z}}{N_{ReR}}\right)\left\{\dfrac{\gamma+1}{B} + e^{2B}\left(-\dfrac{\gamma+1}{B} + 2\gamma - 2B + 2\right)\right\}}{(Be^{2B} - e^{2B} + B + 1)}}{\dfrac{B+1}{\gamma} + e^{2B}\left(\dfrac{B-1}{\gamma}\right)} \tag{3}$$

$$\frac{\partial \Gamma}{\partial \varepsilon} = \frac{\dfrac{\varepsilon B}{2Sc} - \dfrac{B^2\left(\dfrac{N_{Re_z}}{N_{ReR}}\right)\left\{\dfrac{\Gamma+1}{B} + e^{2B}\left(-\dfrac{\Gamma+1}{B} + 2\Gamma - 2B + 2\right)\right\}}{(Be^{2B} - e^{2B} + B + 1)}}{\dfrac{B+1}{\Gamma} + e^{2B}\left(\dfrac{B-1}{\Gamma}\right)} \tag{4}$$

where

$$\varepsilon = 4(\nu z/UR^2)^{\frac{1}{2}} \tag{5}$$

and γ and Γ are the respective temperature and concentration analogues of B.

In order to relate the driving forces previously found to the temperature change in the jet, consider the energy equation for the liquid, assuming that

$$V_{r_l} = 0 \tag{6}$$

and neglecting viscous dissipation:

$$\rho_l c_{p_l} U\left(\frac{\partial \theta_S}{\partial z}\right) = k_l\left[\frac{1}{r}\frac{\partial}{\partial r}\left(r\frac{\partial \theta_S}{\partial r}\right) + \frac{\partial^2 \theta_S}{\partial z^2}\right] \tag{7}$$

where θ_S is a modified surface temperature.

Averaging equation (7) over r gives

$$\rho_l c_{p_l} U\frac{\partial \bar{\theta}_S}{\partial z^2} = k_l\left[\frac{1}{\pi R^2}\int_0^R 2\pi r\left\{\frac{1}{r}\frac{\partial}{\partial r} \times \left(r\frac{\partial \theta_S}{\partial r}\right)\right\}dr + \frac{\partial^2 \bar{\theta}_S}{\partial z^2}\right] \tag{8}$$

where

$$\frac{1}{\pi R^2}\int_0^R 2\pi r\, \Upsilon\, dr = \bar{\Upsilon}. \tag{9}$$

Thus,

$$\rho_l c_{p_l} U\frac{\partial \bar{\theta}_S}{\partial z} = k_l\left[\frac{2}{R}\left(\frac{\partial \theta_S}{\partial r}\right) + \frac{\partial^2 \bar{\theta}_S}{\partial z^2}\right] \tag{10}$$

$\bar{\theta}_S = \theta_S$, since the temperature is assumed constant across the radius of the jet.

If the heat flow in the axial direction in the jet, due to conduction, is negligibly small (valid if the jet is sufficiently thin or its velocity is sufficiently high*) equation (10) becomes

$$\left(\frac{\partial \theta}{\partial r}\right)_{r=R} = \frac{R\rho_l c_{p_l} U}{2k}\left(\frac{\partial \theta_S}{\partial z}\right) - \frac{N_A}{k}\Delta H_V \tag{11}$$

since

$$k_l\left(\frac{\partial \theta_S}{\partial r}\right)_{r=R} = k\left(\frac{\partial \theta}{\partial r}\right) + N_A \Delta H_V. \tag{12}$$

Applying Fick's first law of diffusion in terms of the molar flux relative to stationary coordinates for a binary system at the jet edge gives [15]

$$(N_A)_{y=0} = \frac{-D_{AB}\left(\dfrac{\partial C_A}{\partial y}\right)_{y=0}}{1 - \dfrac{C_{A\,\mathrm{sat}}(T_1)}{c}}, \tag{13}$$

where $C_{A_{\mathrm{sat}}}(T_1)$ is the saturation concentration at the initial jet temperature

If the bulk flow term is neglected, the surface

* i.e. valid if the time required for significant axial conduction is large compared to either or both the residence time and the time necessary for significant radial conduction.

flux is given by

$$N_A = -cD_{AB}\left(\frac{\partial x_A}{\partial y}\right)_{y=0} = -D_{AB}\left(\frac{\partial C_A}{\partial y}\right)_{y=0} = \frac{D_{AB}C_{A_S}}{R\Gamma} \quad (14)$$

since

$$\left(\frac{\partial C_A}{\partial y}\right)_{y=0} = \sim \frac{C_{A_S}}{R\Gamma}. \quad (15)$$

Solving equation (11) for the temperature change with axial distance and putting the equation in non-dimensional form results in:

$$4\left(\frac{\partial \Psi_l}{\varepsilon \partial \varepsilon}\right) = \frac{-\Psi_l}{Pr\left(\frac{\rho_l c_{p_l}}{\rho c_p}\right)\gamma} + \frac{CnQ}{Sc\Gamma}$$

(neglecting bulk flow) (16)

where $Cn = \Delta H_v(c_{Ai} - c_{A\infty})/(\rho_1 c_{p_1})(T_i - T_\infty)$; $Q = (c_A - c_{A\infty})/(c_{Ai} - c_{A\infty})$; and

$$\Psi = (T - T_\infty)/(T_i - T_\infty). \quad (17)$$

The values of γ and Γ appropriate for negligible axial temperature and concentration change and found from the Runge–Kutta solutions of the thermal and concentration equations*, respectively, are substituted in equation (16) to find the surface temperature at a given axial distance. This iterative procedure is valid for small axial temperature change only.

Because $\Gamma = \gamma = 0$ at $\varepsilon = 0$, the terms $\partial\Gamma/\partial\varepsilon$ and $\partial\gamma/\partial\varepsilon$ (see equations (3) and (4)) exhibit singularities here. However, an analytical expression can be found for B in the neighborhood of $\varepsilon = 0$. Assuming that a proportional relationship exists between B and γ and between B and Γ (as $\varepsilon \to 0$), constants of proportionality can be determined by analyzing the expressions for $\partial\Gamma/\partial\varepsilon$ and $\partial\gamma/\partial\varepsilon$ as $\varepsilon \to 0$ (refer to Appendix for details).

The fact that this procedure results in an explicit evaluation of the constants verifies the assumed relationships between B and γ and B and Γ. The relationship was expected since the $\partial\gamma/\partial\varepsilon$ and $\partial\Gamma/\partial\varepsilon$ equations are analogous and obey similar boundary conditions.

Equation (16) was put into universal plot* form by assuming that the variation of γ and Γ with ε is similar (i.e. that the asymptotic value of γ/Γ as $\varepsilon \to 0$ holds, approximately, over all ε). This assumption is reasonable, since the change of γ with axial distance is governed by an equation completely analogous to that which governs the change of Γ, both obeying similar boundary conditions. The assumption was checked on the computer and was found to be valid to within a few per cent. Therefore, equation (16) becomes:

$$\left(\frac{\partial \Psi_l}{\partial \varepsilon^2}\right) = \left\{\frac{-\Psi_l \rho c_p[(2/Sc) + 1]}{Pr\rho_l c_{p_l}[(2/Pr) + 1]} + \frac{CnQ}{Sc}\right\} 8\Gamma. \quad (18)$$

The evaluation procedure used was to integrate equation (18) over small axial increments by assuming constant driving forces and using Simpson's rule.

Thus, the expression for the axial temperature change in the jet has been determined by neglecting the axial temperature and concentration variation at the jet surface in the expression for the driving forces for heat transfer.

The variation of B and Γ, as well as the variation of $1/\Gamma$, which is directly proportional to the mass flux if C_{A_S} is constant, with non-dimensional axial distance is shown in Fig. 2.

A comparison of the local Nusselt number (Nu) variation with non-dimensional axial distance for finite and continuous cylinders in air with constant cylinder temperature is shown in

* Utilizing values of B determined from a correlation of B values from zero to ten as a function of $N_{Re_z}/N^2_{Re_R}$. Refer to [12] for details.

* A universal plot would not have been possible had the bulk flow contribution been included in the theoretical analysis. Its inclusion would not otherwise severely complicate the analysis, however.

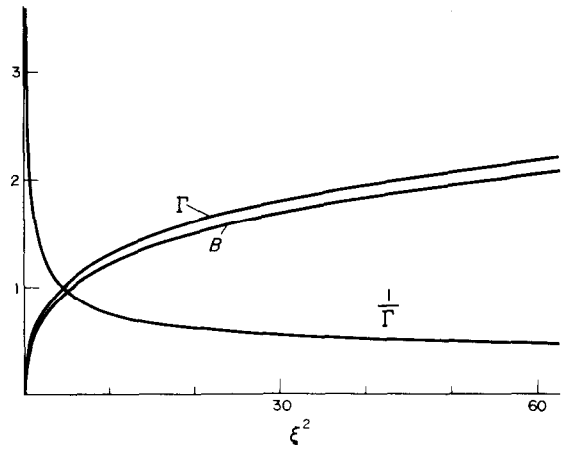

FIG. 2. The variation of the non-dimensional coefficients B, Γ and $1/\Gamma$ with non-dimensional axial distance ε^2.

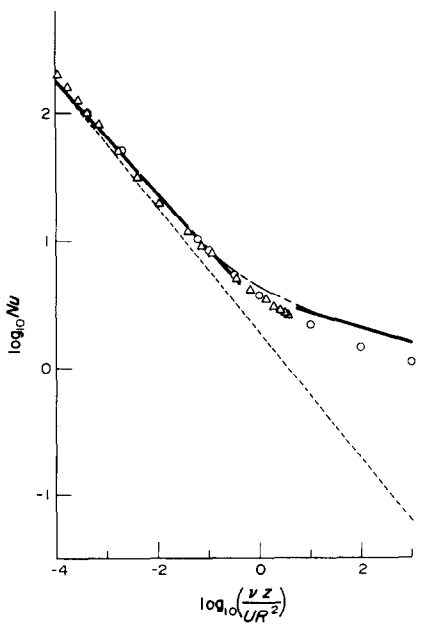

FIG. 3. Comparison of local Nusselt number variation with non-dimensional axial distance for finite and continuous cylinders. Solid lines on left and right and dashed central curve apply for finite cylinders. Circles are Bourne and Elliston's values for continuous cylinders. Triangles are from present work on continuous cylinders. Finite flat plate values are shown as dashed line.

Fig. 3, where

$$Nu = \frac{Q'}{k\theta_S} = \frac{2\pi}{\gamma} \tag{19}$$

and Q' is the rate of heat transfer per unit length.

The finite cylinder solutions are shown as solid curves (the left one being based on the Seban–Bond–Kelly solution, the dashed middle one on Bourne and Davies power law approximation, and the right solid one on the asymptotic solution) [16]. The finite flate plate solution is also shown as a dashed line [16].

The continuous cylinder solutions are shown as points. The present work's values (triangles) are in close agreement with those of Bourne and Elliston [10] (circles). The slight disparity between the two, which would negligibly change the predicted temperature profile, may be due to Bourne and Elliston's technique of including higher order terms in their determination of analytic solutions in the neighborhood of $z = 0$ or to the slightly differing integration procedures.

The value of the local Nusselt number for the continuous cylinder lies above that of the finite cylinder at values of $\log_{10}(vz/UR^2)$ lower that about -3 and below it at higher values, the deviation becoming greater the farther the deviation of the abscissa from $\log_{10}(vz/UR^2) = -3$. This difference, reaches approximately 28 per cent of the finite cylinder value at $\log_{10}(vz/UR^2) = +3$ and approximately 17 per cent at $\log_{10}(vz/UR^2) = -4$.

EXPERIMENTAL TECHNIQUE

The experimental apparatus used to determine the heat transfer to or from a vertical laminar liquid jet ejecting from a reservoir at one temperature into a gas at another temperature is shown in Fig. 1b. The outside chambers of both the lower and upper levels of the apparatus contain temperature controlled water reservoirs. The upper inner chamber is a liquid reservoir, fabricated of glass and modified to maintain an approximately constant head. Between the upper and lower inner sections is a precision

bore glass capillary tube, used to form the jets. The lower inner chamber is a gas bath, fabricated of aluminium with glass windows. It contains a movable Teflon rod, which supports a Teflon mixing cup containing a 0·0075 cm diameter wire thermocouple (0·0113 cm bead) used to measure the jet temperature, and a fine Teflon tube used to obtain vapor samples to be analyzed by chromatography to determine the vapor composition. Initially, sampling was accomplished directly from the Teflon tubing by means of a hypodermic syringe. More reproducible data were later obtained by sampling from a miniature three-way valve equipped with luer-lok fittings to minimize leakage. For a more detailed description of the apparatus, refer to [12].

During a run measurements are taken of the temperature change from the top reservoir as a function of position down the jet by means of a Hewlett–Packard null voltmeter and a Scientific Instruments cathetometer. The gas samples are analyzed on a Beckmann GC-2A gas chromatograph, equipped with a column packed with Poropak Q. An average jet velocity is determined from measurements of the volume of the liquid collected and the time of the run.

The experimental work was carried out with methanol jets, since the chromatograph calibration gave quantitative results for only air and methanol and the heat transfer is critically sensitive to small changes in the vapor composition.

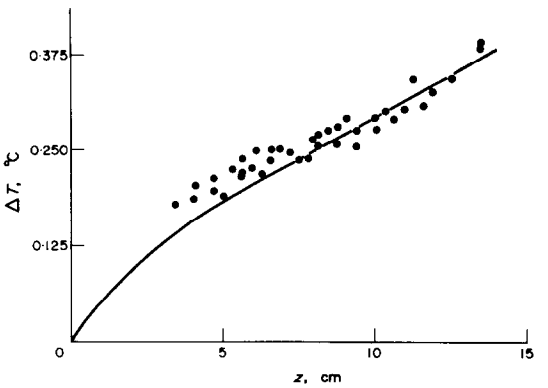

FIG. 4. Axial temperature change variation with axial distance for various heating runs with 0·125 cm capillary diameter methanol jets. Solid curve is theoretical prediction, whereas points represent experimental results (refer to Table 1).

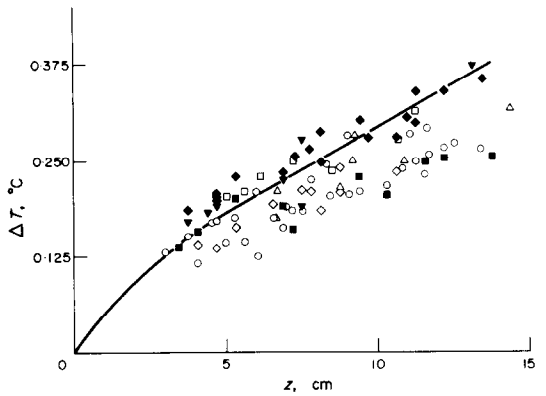

FIG. 5. Axial temperature change variation with axial distance for various heating runs with 0·125 cm capillary diameter methanol jets. Solid curve is theoretical prediction, whereas points represent experimental results (refer to Table 1).

EXPERIMENTAL RESULTS AND DISCUSSION

In the initial experiments (Figs. 4–9) measures were taken to insure that the air bath was either completely saturated or completely unsaturated (by keeping a pool of liquid in the lower portion of the gas bath compartment for long periods of time or by repeated flushing of the gas phase with compressed air, respectively), but no vapor samples were taken for confirmation.

Figures 4–7 show experimental heat transfer data for the methanol–air system (refer to Table 1), using either a completely saturated

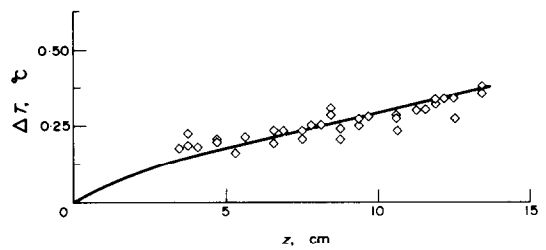

FIG. 6. Axial temperature change variation with axial distance for various heating runs with 0·125 cm capillary diameter for methanol jets. Solid curve is theoretical prediction, whereas points represent experimental results (refer to Table 1).

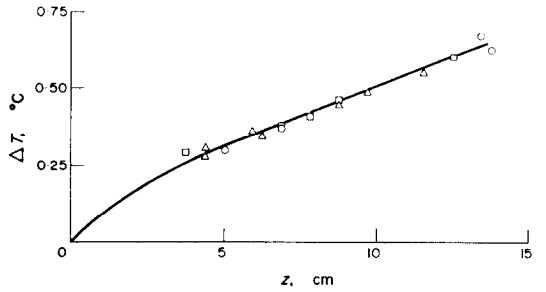

FIG. 7. Axial temperature change variation with axial distance for various cooling runs with 0·125 cm capillary diameter methanol jets. Solid curve is theoretical prediction, whereas points represent experimental results (refer to Table 1).

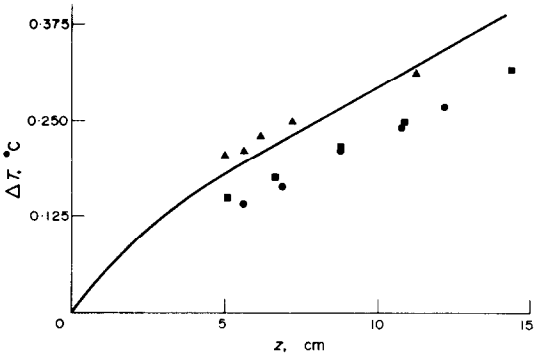

FIG. 8. Temperature change occurring in three heating runs on 0·125 cm dia methanol jets. Solid curve is theoretical prediction for saturated air, while points represent experimental data (refer to Table 1).

or unsaturated air bath and a 0·125 cm dia capillary tube. The predictions of the theory (neglecting bulk flow at the jet surface but assuming an initially saturated air bath for heating runs and an initially unsaturated air bath for cooling runs in order to predict maximum temperature changes) are shown in these figures as solid curves.

Figure 8 compares equations (18) for saturated air with experimental data from three methanol runs utilizing 0·125 cm dia jets with $U = 96{\cdot}3$ cm/s, $T_B = 25{\cdot}0\,^{\circ}C$ and $\Delta T = 10{\cdot}0\,^{\circ}C$. The data seem to fall on curves parallel to the theoretical curve, but are displaced from it to varying degrees, probably due to changing vapor saturation and surface bulk flow.

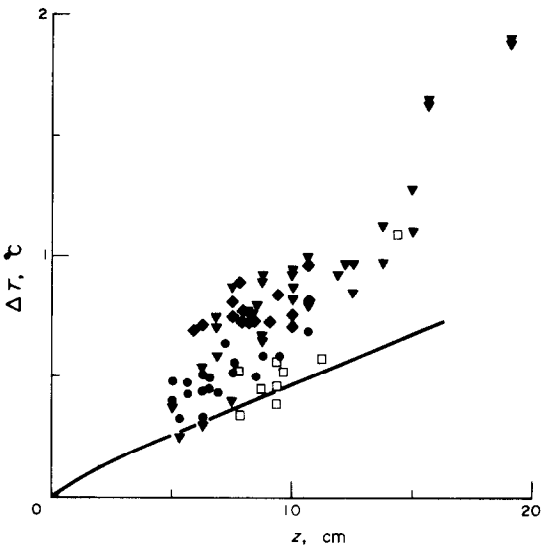

FIG. 9. Temperature change occurring in several heating runs on 0·075 cm dia methanol jets. Solid curve is theoretical prediction for saturated air, while points represent experimental results (refer to Table 1).

Figure 9 depicts the lack of agreement between experiment and theory for a 0·075 cm dia jet where instabilities have set in at small distances down the jet. The theoretical curve is shown for one set of conditions only, whereas the data were taken at various velocities and temperatures. The closest agreement between experiment and theory is found when similar velocity jets are compared. Slower jets show higher temperature changes, as the theory would predict. At similar bath temperature differentials, experimental temperature changes are higher than those predicted in all cases. This disparity is believed due to the non-stationary flow observed in these experiments. The gravity flow method used in the previous experiments with 0·125 cm dia tubes only produced dribbling jets with smaller diameter tubes. Producing a continuous jet with such small diameter capillary tubes required nitrogen gas pressure. This resulted in turbulent jets, which as expected showed greater heat transfer than would be the case for laminar jets.

Since Fig. 8 casts doubt whether complete

Table 1. Relevant parameters for and designation of the runs depicted in Figs 4–12

Figure	Run designation	Diameter (cm)	Velocity (cm/s)	T_B (°C)	$T_T - T_B$ / ΔT (°C)	% Saturation
4, 5, 6, 8	——	0·125	96·0	24·7	− 10·0	100
4	●	0·125	96·3	25·0	− 10·0	
5	♦			24·3	− 10·3	
	◇			25·0	− 10·2	
	▼			24·6	− 10·1	
	△			23·7	− 10·0	
	○			24·0	− 9·8	
	□			24.2	− 9·8	
	■			24·2	− 9·7	
6	◇			25·0	− 10·1	
7	——	0·125	96·0	13·0	+ 10·0	0
	○	0·125	94·2	13·2	+ 13·1	
	□			13.2	+ 12·7	
	△			15·6	+ 10·7	
8	△○□	0·125	96·3	25·0	− 10·0	
9	——	0·075	165·0	25·0	− 10·0	100
	●	0·075	125·7	24·2	− 14·8	
	■		180·9	23·6	− 16·0	
	♦		77·7	24·8	− 13·6	
	▼		78·0	25·0	− 15·0	
10	■	0·125	132·0	16·6	+ 9·8	45
11	■	0·125	132·0	18·7	+ 10·4	45
12	1 ○			23·0	+ 10·1	55
	2, 1 □			24·0	+ 11·4	63
	2,2 ●			25·0	+ 14·1	55
	7,1 △			18·1	+ 7·8	60
	7,2 ▽			18·6	+ 7·3	72
	8,1 ◇			16·7	+ 9·6	50
	8,2 ■			17·8	+ 8·5	78
	10,1 ▲			17·4	+ 3·0	70
	10,2 ♦			16·3	− 4·3	95
	12,1 ▼			22·2	+ 3·7	91

vapor saturation was being achieved, the vapor saturation was experimentally determined during each of the runs depicted in Figs. 10–12.

Figures 10 and 11 show comparisons between the theoretical predictions of equation (18) and the experimental results. Figure 10 shows the marked influence the evaporative process has on the heat transfer, completely dominating the convective-conductive effect.

Because the phase change occurring has such a dominant influence on the heat transfer characteristics of the flow, it is important to point out the following:

(1) A relatively small error in determining the vapor composition, will have a large effect on

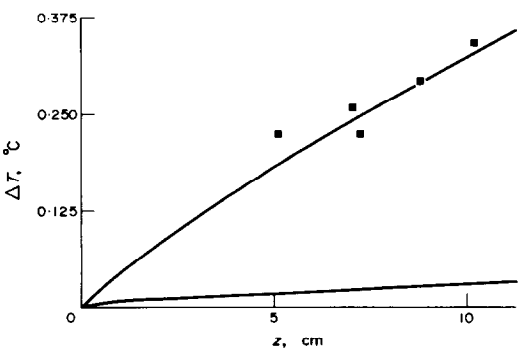

FIG. 10. Axial temperature change with axial distance for 0·125 cm dia methanol jets. Solid curves are theoretical predictions, while points represent experimental results. Lower solid curve represents theoretical prediction neglecting phase change effect (refer to Table 1).

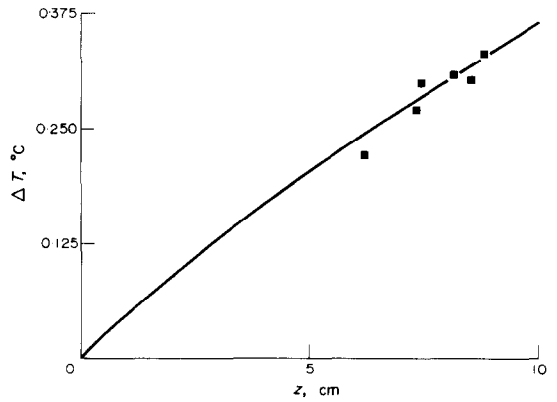

FIG. 11. Axial temperature change with axial distance for 0·125 cm dia methanol jets. Solid curve is theoretical prediction, while points represent experimental results (refer to Table 1).

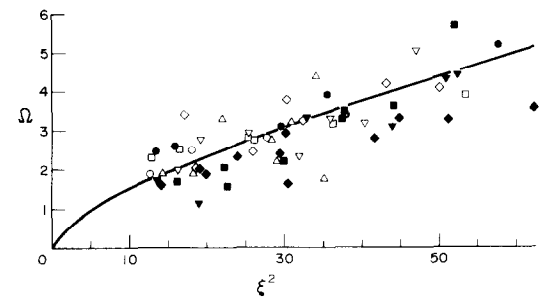

FIG. 12. Nondimensional temperature change variation with nondimensional axial distance for cooling and heating runs with 0·125 cm dia methanol jets. Solid curve is theoretical prediction, while points represent bulk flow corrected results (refer to Table 1). Data from run 10.1 omitted.

the predicted heat transfer. (This is especially true for heating runs, wherein such an error could lead to condensation being predicted while, in reality, evaporation occurs.) (2) If the vapor composition is not initially uniform, error is introduced into the analysis (the vapor composition is undoubtedly non-uniform, due to evaporation from the pool that collects at the bottom of the jet chamber during a run or, possibly, is left in the chamber bottom to increase the vapor saturation), and (3) If the vapor composition is substantially changed during the course of a run, significant error is introduced (this occurrence is unavoidable, but may be minimized by short experimental runs and by careful choice of initial vapor compositions to minimize evaporation or condensation i.e. close to saturation at the gas bath temperature for cooling runs or close to the saturated vapor composition at the initial temperature of the jet, for heating runs, where little temperature change in the jet is expected).

Equation (18) affords the possibility of a universal plot and should be accurate, since the temperature changes down the jet are usually small (a maximum of one and a half degrees C).

The theoretical prediction, neglecting the bulk flow term, is in general agreement with the experimental results for cooling runs and for heating runs for which condensation was predicted. For heating runs, when evaporation was predicted, however, the data were highly dispersed. No confirmation of the theory could be found for this case. Lack of knowledge of the vapor composition throughout the experimental vapor volume was probably the main cause of the discrepancy.

The predicted cooling during a "heating" run, caused by evaporative transfer being the dominant heat transfer mechanism, was observed several times at low temperature differences between the liquid and gas baths. The agreement with the theory was not quantitative, however, due to sensitivity to the experimentally-determined value of the vapor composition.

Even for the cooling case, the data were scattered around the theoretical prediction. Possible reasons for this include the following:

(1) Unsteady-state behavior (the jet temperature at a given height varies slightly during the course of a run, possibly due to changes in the vapor composition) (2) Initial non-uniform vapor composition, (3) Water vapor in the air. (The amount of methanol in the vapor was usually about ten times the amount of water present, an amount which varies from day to day. The effect of a third component is not considered in the analysis, but could be reflected in the amount of methanol present in the vapor,

in the rate of methanol diffusion to or from the jet surface, and in possible water condensation on the jet.) (4) Non-uniform temperature profile across the radius of the jet (at best, gradients are expected near the jet surface), and (5) Non-negligible bulk flow contribution to the heat transfer.

Considering the assumptions involved, the agreement between experiment and theory is considered to be satisfactory. In cases where there is disagreement, the data usually fall on curves parallel to the theoretical one, suggesting inaccuracy in the determination of the vapor composition (and/or a significant bulk flow contribution). It is extremely difficult to accurately sample vapor compositions in a stagnant gas phase.

When the error involved in the bulk flow assumption is calculated for each run, it becomes apparent that this contribution alone may account for much of the scatter in the data. The closeness of the agreement of the data with the theoretical prediction (neglecting bulk flow at the surface) shows a strong correlation with the error involved in making this assumption. Except for run 10, 1, for which the vapor saturation may not be accurate, the lower the error made in neglecting bulk flow, the closer is the agreement between experiment and theory. The closest agreement is found for run 12,1, for which the error involved in neglecting bulk flow is the least. The largest disparity between experiment and theory is found in run 2,2, for which this error is a maximum. Since neglecting bulk flow reduces the predicted temperature change—i.e. bulk flow increases the amount of heat transfer—the experimental results are displaced from the theoretical in the expected direction.

A measure of the effect of bulk flow (relative to the Reynolds flux) is given by the parameter b [17]

$$b = \frac{m_{M,g} - m_{M,s}}{m_{M,s} - 1} \approx \frac{x_{M,g} - x_{M,s}}{x_{M,s} - 1}$$

for air and methanol . (20)

Thus, it is possible to approximately correct the experimental non-dimensional temperature changes by dividing by $(1 + b)$ to determine the expected axial temperature change in the absence of bulk flow.

If the indicated bulk flow correction is made on the data from the runs for which this effect is largest (22·4–34·0 per cent), Fig. 12 results, where

$$\Omega = \Delta\theta/\theta_i\chi \tag{21}$$

and

$$\chi = \frac{\rho c_p [(2/Sc) + 1]}{\rho_l c_{p_l} Pr [(2/Pr) + 1]} + \frac{\Delta H_V (c_{A_i} - c_{A_\infty})}{Sc\rho_l c_{p_l}\theta_i}. \tag{22}$$

Closely analyzing these result, the following is found:

(1) The agreement between experiment and theory is generally satisfactory (2) In some cases, the data drop below the theory at high values of ε^2, probably due to varying initial vapor composition with axial distance, or to the increasing inaccuracy in the assumption of small jet temperature change, and (3) Some of the runs yielded data with a larger amount of scatter than normal (especially runs 7,1 and 7,2), possibly caused by insufficient temperature equilibration in the liquid or in the gas, resulting in natural convection. The data from cooling run 10,1 fall significantly below the theoretical curve by 30–40 per cent, possibly due to error in the chromatographic vapor composition determination and are omitted from Fig. 12.

Final experimentation was limited to one capillary diameter (0·125 cm), since use of larger diameters renders the assumption of constant temperature profile in the radial direction suspect and use of smaller diameters requires a gas pressure head (which tends to produce stable jets over only a small range of velocities) in addition to the liquid head, which alone is sufficient for 0·125 cm dia jets.

Experimental temperature change measure-

ments on the 0·188 cm dia methanol jet yielded low results relative to the theoretical prediction; while measurements on the 0·075 cm dia methanol jet showed characteristically high and inconsistent (possibly due to the instabilities in the jet) results, relative to the theory. For both diameters, however, the experimental results were within a factor of three of the predicted values.

CONCLUSION

The approximate integral solution to the problem of heat transfer in the laminar boundary layer on a constant surface temperature continuous cylinder may be applied to determine the axial temperature profile in a thin, volatile laminar liquid jet undergoing a small temperature change.

ACKNOWLEDGEMENTS

The authors would like to thank the National Science Foundation for its support of this work under grant NSF-GK-3204. One of the authors (RDK) would like to thank the National Aeronautics and Space Administration for its traineeship support.

REFERENCES

1. B. C. SAKIADIS, Boundary-layer behavior on continuous solid surfaces: I. Boundary-layer equations for two-dimensional and axisymmetric flow, *A.I.Ch.E. Jl* **7**, 26–28 (1961).
2. B. C. SAKIADIS, Boundary-layer behavior on continuous solid surfaces: III. The boundary layer on a continuous cylindrical surface, *A.I.Ch.E. Jl* **7**, 467–472 (1961).
3. E. A. KOLDENHOFF, Laminar boundary layers on continuous flat and cylindrical surfaces, *A.I.Ch.E. Jl* **9**, 411–418 (1963).
4. R. M. GRIFFITH, Velocity, temperature, and concentration distributions during fiber spinning, *I/EC Fundamentals* **3**, 245–250 (1964).
5. L. E. ERICKSON, L. C. CHA and L. T. FAN, The cooling of a moving continuous flat sheet, *Chem. Engng Prog. Symp. Ser.* No. 64, **62**, 157–165 (1966).
6. L. E. ERICKSON, L. T. FAN and V. G. FOX, Heat and mass transfer on a moving continuous flat plate with suction or injection, *I/EC Fundamentals* **5**, 19–25 (1966).
7. F. K. TSOU, E. M. SPARROW and R. J. GOLDSTEIN, Flow and heat transfer in the boundary layer on a continuous moving surface, *Int. J. Heat Mass Transfer* **10**, 219–235 (1967).
8. J. W. ROTTE and W. J. BEEK, Some models for the calculation of heat transfer coefficients to a moving continuous cylinder, *Chem. Engng Sci.* **24**, 705–716 (1969).
9. J. W. ROTTE, L. J. TUMMERS and J. L. DEKKER, Mass transfer to a moving continuous cylinder, *Chem. Engng Sci.* **24**, 1009–1015 (1969).
10. D. E. BOURNE and D. G. ELLISTON, Heat transfer through the axially symmetric boundary layer on a moving circular fibre, *Int. J. Heat Mass Transfer* **13**, 583–593 (1970).
11. S. MIDDLEMAN and G. VASUDEVAN, Momentum, heat, and mass transfer to a continuous cylindrical surface in axial motion, *A.I.Ch.E. Jl* **16**, 614–619 (1970).
12. R. D. KAPLAN, Homogeneous nucleation in a liquid miscibility gap system, dissertation, Yale University (1970).
13. J. R. MAA, Evaporation coefficient of liquids, *I/EC Fundamentals* **6**, 504–518 (1967).
14. S. MIDDLEMAN and J. GAVIS, Expansion and contraction of capillary jets of Newtonian liquids, *Physics Fluids* **4**, 355–359 (1961).
15. R. B. BIRD, W. E. STEWART and E. N. LIGHTFOOT, *Transport Phenomena*, p. 83, 85, 319, 502. John Wiley, New York (1964).
16. D. E. BOURNE and D. R. DAVIES, Heat transfer through the laminar boundary layer on a circular cylinder in axial incompressible flow, *Q. J. Mech. Appl. Math.* **XI**, Part 1, 52–66 (1958).
17. D. B. SPALDING, *Convective Mass Transfer*. McGraw-Hill, New York (1963).

APPENDIX

Determination of Analytical Solutions for the Non-dimensional Coefficients β, γ and Γ near $z = 0$

In order to find analytical solutions for the coefficients β γ, and Γ valid near $z = 0$, the following form of equation (1) is used:

$$\frac{\partial B}{\partial z} = \frac{2B^2 v}{UR^2(Be^{2B} - e^{2B} + B + 1)} = \frac{KB^2}{Be^{2B} - e^{2B} + B + 1} \tag{A.1}$$

where

$$K = \frac{2v}{UR^2}. \tag{A.2}$$

Since

$$e^{2B} = 1 + 2B + \frac{(2B)^2}{2!} + \frac{(2B)^3}{3!} + \ldots = 1 + 2B + 2B^2 + \tfrac{4}{3}B^3 + \ldots \tag{A.3}$$

equation (A.1) becomes:

$$\frac{\partial B}{\partial z} = \frac{KB^2}{B(+2B + 2B^2 + \frac{4}{3}B^3) - (1 + 2B + 2B^2 + \frac{4}{3}B^3) + B + 1}$$

and

$$= \left(\frac{\partial B}{\partial z}\right)_{B\to 0} \qquad \frac{KB^2}{\frac{2}{3}B^3 + \frac{4}{3}B^4} = \frac{KB^2}{\frac{2}{3}B^3} = \frac{3K}{2B} \tag{A.4}$$

$$\int_0^B B\,\partial B = \int_0^z \frac{3K}{2}\,\mathrm{d}z.$$

Integrating,

$$B = (3Kz)^{\frac{1}{2}} = \left(\frac{6\nu z}{UR^2}\right)^{\frac{1}{2}} = \frac{(6N_{Re_z})^{\frac{1}{2}}}{N_{Re_R}} \tag{A.5}$$

Substituting equation (A.2) in equation (A.4) gives:

$$\left(\frac{\partial B}{\partial z}\right)_{B\to 0} = \frac{3\nu}{UR^2 B}. \tag{A.6}$$

Equation (3) may be written as:

$$\left(\frac{\partial \gamma}{\partial z}\right) = \frac{\frac{4\alpha B}{UR^2} - \frac{2B^2\nu}{UR^2}\dfrac{\dfrac{\gamma+1}{B} + \mathrm{e}^{2B}\left(2\gamma - 2B + 2 - \dfrac{\gamma+1}{B}\right)}{B\mathrm{e}^{2B} - \mathrm{e}^{2B} + B + 1}}{\dfrac{1}{\gamma}(1 + B + \mathrm{e}^{2B}\{B-1\})} \tag{A.7}$$

(for $Pr \leqslant 1$)

$$B\mathrm{e}^{2B} - \mathrm{e}^{2B} + B + 1 \to \tfrac{2}{3}B^3$$

(refer to equation (A.4). Using equation (A.3):

$$\frac{\gamma+1}{B} + (1 + 2B + 2B^2 + \tfrac{4}{3}B^3)\left(2\gamma - 2B + 2 - \frac{\gamma+1}{B}\right)$$
$$= \left(\frac{\gamma+1}{B}\right) + 2\gamma - 2B + 2 - \left(\frac{\gamma+1}{B}\right)$$
$$+ 4B\gamma - 4B^2 + 4B - 2\gamma - 2 + 4B^2\gamma - 4B^3$$
$$+ 4B^2 - 2B\gamma - 2B + \tfrac{8}{3}B^3\gamma - \tfrac{8}{3}B^4 + \tfrac{8}{3}B^3 - \tfrac{4}{3}B^2\gamma - \tfrac{4}{3}B^2$$
$$= 4B\gamma + 4B^2\gamma - 4B^3 - 2B\gamma + \tfrac{8}{3}B^3\gamma - \tfrac{8}{3}B^4 + \tfrac{8}{3}B^3$$
$$-\tfrac{4}{3}B^2\gamma - \tfrac{4}{3}B^2 = 2B\gamma - \tfrac{4}{3}B^2 \tag{A.8}$$

(to the lowest order terms).

Thus, using the last two results,

$$\left(\frac{\partial \gamma}{\partial z}\right)_{B,\,\gamma\to 0} = \frac{3\gamma}{UR^2}\frac{(2\alpha B - 3\nu(\gamma - \frac{2}{3}B))}{B^3} \tag{A.9}$$

setting

$$B_{z\to 0} = C\gamma_{z\to 0}. \tag{A.10}$$

Then

$$\left(\frac{\partial B}{\partial z}\right)_{z\to 0} = C\left(\frac{\partial \gamma}{\partial z}\right)_{z\to 0} \tag{A.11}$$

Substituting equations (A.6), (A.9) and (A.10) in equation (A.11) gives:

$$\frac{3(\nu/UR^2)}{C\gamma} = \frac{C(3\gamma)}{(UR^2)}\frac{2\alpha C\gamma - 3\nu(\gamma - \frac{2}{3}C\gamma)}{(C\gamma)^3}$$

or

$$1 = 2\left(\frac{1}{Pr}\right) - \frac{3}{C} + 2,$$

where $Pr = \nu/\alpha$.

Thus,

$$C = \frac{3}{[(2/Pr) + 1]}. \tag{A.12}$$

Similarly, (refer to equation (4))

$$\left(\frac{\partial \Gamma}{\partial z}\right)_{z\to 0} = \frac{3\Gamma}{B^3 UR^2}\,[2D_{AB}B - 3\nu(\Gamma - \tfrac{2}{3}B)]$$

$$B_{z\to 0} = D\Gamma_{z=0} \tag{A.13}$$

$$\left(\frac{\partial B}{\partial z}\right)_{z\to 0} = D\left(\frac{\partial \Gamma}{\partial z}\right)_{z\to 0}$$

and

$$D = \frac{3}{[(2/Sc) + 1]},$$

where $Sc = \nu/D_{AB}$.

From equation (A.12):

$$\frac{2}{Pr} + 1 = \frac{3}{C}$$

or

$$Pr = \frac{2}{\frac{3}{C} - 1}$$

as $Pr \to 0$

$$Pr_{\to 0} = \frac{2C}{3}$$

or

$$C_{Pr\to 0} = \frac{3Pr}{2}. \tag{A.14}$$

Thus, from equations (A.10) and (A.14):

$$\left(\frac{\gamma}{B}\right)_{Pr\to 0} = \frac{1}{C} = \frac{2}{3Pr}. \tag{A.15}$$

For $Pr \leqslant 1$, Rotte and Beck [8], derived (for the continuous cylinder)

$$\left(\frac{\gamma}{B}\right)_{z\to 0} = \frac{2 + Pr}{3Pr}$$

or

$$\left(\frac{\gamma}{B}\right)_{Pr\to 0} = \frac{2}{3Pr}$$

in agreement with the above.

TRANSFERT THERMIQUE A UN JET LAMINAIRE CYLINDRIQUE DE LIQUIDE DANS UN GAZ

Résumé—Le transfert thermique expérimentalement déterminé pour un jet vertical et cylindrique laminaire de liquide envoyé dans une ambiance gazeuse—où la résistance au transfert thermique dans la phase gazeuse est contrôlée—est comparé à celui estimé par la technique de Pohlhausen–Von Karman en utilisant des profils logarithmiques pour résoudre les équations de diffusion de masse, de quantité de mouvement et d'énergie.

La solution théorique a été obtenue pour le cas d'un débit global négligeable à la surface (comparé aux flux de Reynolds), d'une conduction thermique radiale rapide, et d'un faible changement de température du jet. Elle est en accord avec les résultats expérimentaux, pourvu que le rayon du jet soit suffisamment petit. On montre que la solution, qui comprend l'effet d'évaporation et de condensation, peut être mise sous la forme d'une représentation universelle du changement de la température axiale adimensionnelle en fonction de la distance axiale adimensionnelle.

WÄRMEÜBERGANG AN EINEM ZYLINDRISCHEN LAMINAREN FLÜSSIGKEITSSTRAHL, DER IN EIN GAS AUSSTRÖMT

Zusammenfassung—Der experimentell bestimmte Wärmeübergang an einem vertikalen zylindrischen laminaren Flüssigkeitsstrahl, der in ein umgebendes Gas ausströmt, wobei der Wärmeübergangswiderstand in der Gasphase geschwindigkeitsbestimmend ist, wird verglichen mit dem nach der Pohlhausen- von Kàrmàn Technik vorausgesagten. Logarithmische Profile werden benützt zur Lösung der Kontinuitäts-, Bewegungs-, Energie- und Diffusionsgleichung. Die theoretische Lösung wurde für den Fall vernachlässigbarer Viskosität (verglichen mit der Reynoldsströmung) an der Oberfläche abgeleitet, ferner für schnelle radiale Wärmeleitung und kleiner Strahltemperaturänderung. Es ergab sich Übereinstimmung mit experimentellen Daten, wenn der Strahlradius genügend klein war. Es wird gezeigt, dass die Lösung, welche die Effekte der Verdampfung oder Kondensation einschliesst, in eine universelle Form gebracht werden kann, in einem Diagramm mit dimensionsloser Axialtemperaturänderung zu dimensionslosem Achsabstand.

ПЕРЕНОС ТЕПЛА К ЦИЛИНДРИЧЕСКОЙ ЛАМИНАРНОЙ ЖИДКОЙ СТРУЕ, ВДУВАЕМОЙ В ГАЗ

Аннотация—Экспериментальные данные по теплообмену при вдуве вертикальной цилиндрической ламинарной струи жидкости в газовую камеру, когда варьируемым параметром было сопротивление переносу тепла в газовой фазе, сравниваются с расчетами по методу Кармана-Польгаузена с логарифмической аппроксимацией профилей в уравнениях неразрывности, импульса, энергии и диффузии.

Полученное аналитическое решение задачи для случая пренебрежимо малого потока в объеме (по сравнению с потоком Рейнольдса) вблизи поверхности, интенсивной теплопроводности в радиальном направлении и малого изменения температуры струи согласуется с экспериментальными данными для струй с малым радиусом. Решение с учетом вклада испарения или конденсации может быть представлено в виде универсальной зависимости изменения безразмерной температуры по оси от безразмерного осевого расстояния.